

Nucleation and growth of helium bubble at (110) twist grain boundaries in tungsten investigated by molecular dynamics

Fang-Biao Li(李芳镖), Guang Ran(冉广), Ning Gao(高宁), Shang-Quan Zhao(赵尚泉), Ning Li(李宁)
Citation: Chin. Phys. B . 2019, 28(8): 085203 . **doi:** 10.1088/1674-1056/28/8/085203
Journal homepage: http://cpb.iphy.ac.cn; http://iopscience.iop.org/cpb

What follows is a list of articles you may be interested in

Numerical study of influence of *J*×*B* force on melt layer under conditions relevant to ITER ELMs

Yan Huang(黄艳), Ji-Zhong Sun(孙继忠), Juan Cai(蔡娟), Zhen-Yue Sun(孙振月), Chao-Feng Sang(桑超峰), De-Zhen Wang(王德真)
Chin. Phys. B . 2019, 28(4): 045201 . **doi:** 10.1088/1674-1056/28/4/045201

Radiative divertor behavior and physics in Ar seeded plasma on EAST

Jingbo Chen(陈竞博), Yanmin Duan(段艳敏), Zhongshi Yang(杨钟时), Liang Wang(王亮), Kai Wu(吴凯), Kedong Li(李克栋), Fang Ding(丁芳), Hongmin Mao(毛红敏), Jichan Xu(许吉禅), Wei Gao(高伟), Ling Zhang(张凌), Jinhua Wu(吴金华), Guang-Nan Luo(罗广南), EAST Team
Chin. Phys. B . 2017, 26(9): 095205 . **doi:** 10.1088/1674-1056/26/9/095205

Tungsten ion source under double-pulse laser ablation system

Ahmed Asaad I Khalil, Ashraf I Hafez, Mahmoud E Elgohary, Mohamed A Morsy
Chin. Phys. B . 2017, 26(9): 095201 . **doi:** 10.1088/1674-1056/26/9/095201

X-ray spectra of high temperature tungsten plasma calculated with collisional radiative model

Wang Jun, Zhang Hong, Cheng Xin-Lu
Chin. Phys. B . 2013, 22(8): 085201 . **doi:** 10.1088/1674-1056/22/8/085201

Radiation characteristics and implosion dynamics of tungsten wire array Z-pinches on the YANG accelerator

Huang Xian-Bin,Yang Li-Bing,Li Jing,Zhou Shao-Tong,Ren Xiao-Dong,Zhang Si-Qun,Dan Jia-Kun,Cai Hong-Chun,Duan Shu-Chao,Chen Guang-Hua,Zhang Zheng-Wei,Ouyang Kai,Li Jun,Zhang Zhao-Hui,Zhou Rong-Guo,Wang Gui-Lin
Chin. Phys. B . 2012, 21(5): 055206 . **doi:** 10.1088/1674-1056/21/5/055206

Nucleation and growth of helium bubble at (110) twist grain boundaries in tungsten studied by molecular dynamics*

Fang-Biao Li(李芳镖)[1], Guang Ran(冉广)[1,†], Ning Gao(高宁)[2,3,‡], Shang-Quan Zhao(赵尚泉)[1], and Ning Li(李宁)[1]

[1] *College of Energy, Xiamen University, Xiamen* 361102, *China*
[2] *Institute of Modern Physics, Chinese Academy of Sciences, Lanzhou* 73000, *China*
[3] *School of Nuclear Science and Technology, University of Chinese Academy of Sciences, Beijing* 100094, *China*

(Received 23 January 2019; revised manuscript received 6 June 2019; published online 25 July 2019)

Migration of He atoms and growth of He bubbles in high angle twist grain boundaries (HAGBs) in tungsten (W) are investigated by atomic simulation method. The energy and free volume (FV) of grain boundary (GB) are affected by the density and structure of dislocation patterns in GB. The migration energy of the He atom between the neighboring trapping sites depends on free volume along the migration path at grain boundary. The region of grain boundary around the He bubble forms an ordered crystal structure when He bubble grows at certain grain boundaries. The He atoms aggregate on the grain boundary plane to form a plate-shape configuration. Furthermore, high grain boundary energy (GBE) results in a large volume of He bubble. Thus, the nucleation and growth of He bubbles in twist grain boundaries depend on the energy of grain boundary, the dislocation patterns and the free volume related migration path on the grain boundary plane.

Keywords: tungsten, dislocation patterns, ordered grain boundary structure, plate-shape He bubble

PACS: 52.65.Yy, 66.30.J–, 61.72.Mm, 66.30.–h **DOI:** 10.1088/1674-1056/28/8/085203

1. Introduction

Because of high melting point, high thermal conductivity, low sputtering rate and low tritium retention rate, tungsten (W) and W-alloys have been selected as the leading candidates for plasma-facing materials (PFMs) in future fusion reactors.[1–3] Although many studies have been performed with different experimental and theoretical methods, there are still many challenges in their future applications. For example, the surface of tungsten will be damaged by irradiation of high-concentration He^+ particles, resulting in the change of structure and hardness of tungsten surface with different crystal orientations.[4,5] Furthermore, because of the extremely low solubility of helium (He) atoms in metallic materials, He atoms generated through (n,α) reaction will migrate, gather and grow to form gas bubbles in metallic materials. Especially, He atoms tend to agglomerate in the dislocation and grain boundary (GB) regions of structural materials which may cause swelling, hardening and high-temperature embrittlement, degrading the service performance and life time of material.[6–8] Therefore, the study of He nucleation and growth in tungsten grain boundary is very important and necessary.

From previous studies, many experiments have been performed to investigate the nucleation of He in the grain boundary (GB).[9–11] The behaviors, sizes, geometries and distributions of He bubbles have also been investigated at different grain boundaries with an *in situ* method.[9] Furthermore, solid helium bubbles were directly observed in the helium ion implanted tungsten by different transmission electron microscopy (TEM) techniques at room temperature.[10] However, it is still very difficult to follow the initial nucleation and growth process of He bubbles *in situ* with the present experimental techniques because of their small size (*e.g.*, less than 10 nm in diameter[11,12]) and fast kinetic process with very low migration energy of interstitial He atoms.[13] As complementary methods, computer simulations have been proved to be useful to predict the changes of the material on different time and length scales, providing a new understanding of the experimental results.[14] Therefore, the extensive studies focusing on the basic properties of GBs and He bubbles have also been conducted by numerical simulations. For example, tensile response of irradiated symmetric grain boundaries to the externally applied strain has been studied by atomic simulation methods.[15] Bai *et al.*[16] found that grain boundaries have a surprising "loading-unloading" effect which can absorb interstitials and re-emit them to annihilate bulk vacancies. Chen *et al.*[17] used molecular statics to explore the energetics of vacancy segregation in a range of equilibrium and metastable [100] symmetric tilt GBs. Furthermore, Valles *et al.*[18] studied the influence of a high GB density on the amount, size and distribution of the defects produced by pulsed He^+ irradiation in the tungsten and revealed that the He atoms retained at GBs increase with the GB density increasing. The preferential nu-

*Project supported by the National Natural Science Foundation of China (Grant Nos. 11305136, 11675230, 11375242, and U1832112).
†Corresponding author. E-mail: gran@xmu.edu.cn
‡Corresponding author. E-mail: ning.gao@impcas.ac.cn
© 2019 Chinese Physical Society and IOP Publishing Ltd

cleation of He bubbles at low-angle grain boundaries in Au and Cu has been studied by the combination of the molecular statics, molecular dynamics and experiments.[7,19] The twist grain boundary (TGB) was also studied for understanding the helium effect on the material, especially for the interaction between the TGB and He atoms.[20,21] Wang *et al.*[22] investigated the segregation, trapping and diffusion of He in a $\Sigma3\langle110\rangle\{111\}$ W grain boundary by the combination techniques of *ab initio* and classical atomistic simulations. Feng *et al.*[23] investigated the grain boundary energy (GBE) of (110) twist grain boundaries and analyzed the dislocations in low-angles grain boundaries. They also investigated the migration and nucleation of He clusters in (110) twist grain boundaries with different angles.[24]

According to previous analysis,[24] (110) TGBs can be divided into low-angle grain boundaries (LAGBs) and high-angle grain boundaries (HAGBs). HAGBs can be further divided into the sub-types: boundaries with low grain boundary energy (LGBEs, *e.g.*, $\Sigma3\theta = 70.53^\circ$) and high grain boundary energy (HGBEs, *e.g.* $\theta = 20^\circ$, $\theta = 40^\circ$), respectively.

Although a lot of studies have been performed as mentioned above, the initial nucleation of He bubble at HAGB in the tungsten is still not studied enough, especially for the case with large-sized bubbles. Related with these grain boundaries, one important question is how the interface structure affects the migration of He atoms and the nucleation of the large-sized He bubbles. Therefore, in the present work, we focus on the migration of He atoms and the nucleation behavior of He bubbles at HAGBs ($\theta = 20^\circ$, $\theta = 40^\circ$, $\theta = 70.53^\circ$) in the tungsten to provide an answer to above question. The rest of this paper is organized as follows. The simulation method is described in Section 2. The grain boundary structure and the energy are analyzed in Subsection 3.1. The migration of He atoms, the change of grain boundary structure and the nucleation of the He bubbles are presented in Subsections 3.2, 3.3, and 3.4 respectively. Finally, the conclusions are drawn from the present study in Section 4.

2. Methods

In this work, the model of twist grain boundary created by Atomsk is used,[25] whose details have been described elsewhere.[23,26] For convenience, the X, Y, and Z axes of the simulation box are set to be in the directions of [-111], [1-12], and [110] respectively. Periodic boundary conditions are applied to the x and y directions, while a fixed boundary condition is used along the z direction. The simulation model of 100 Å×100 Å×180 Å, containing about 1.1×10^5 tungsten atoms is constructed to eliminate the possible size effect.[27] The simulations are performed by the parallel MD code, LAMMPS.[28] The W–He, He–He, and W–W interatomic potential (SNAP potential) have been described in detail in Refs. [29] and [30]. The lattice constant and elastic constants calculated by the interatomic potential are shown in Table 1. From Ref. [30], it is clear that the properties calculated by the SNAP potential are very close to those calculated by density functional theory (DFT), which indicates that the SNAP potential provides a good description for the W–He interaction. After the initial molecular static relaxation, the model is then relaxed under constant number of atoms N, pressure P, and temperature T (NPT) (300 K, 0 Pa) ensemble for 10 ps to release the local highly local stress and disordered structure, finally a thermodynamic equilibrium is reached. The migration of He atoms and the nucleation of He bubbles are investigated through two simulations. In the first simulation, the nudged elastic band (NEB) method is used to analyze the migration energy barrier of He atom in HAGB. In the second simulation, the nucleation processes of He bubbles in HAGBs with different rotation angles are performed at a temperature of 300 K. Firstly, a He atom is introduced into the dislocation-junction of GB as the initial nucleation site, then the system is relaxed to an equilibrium state. After full relaxation, more He atoms are introduced one by one into the bubble by manually placing the He atom within about one lattice constant to the existing He-bubble. Because of the high binding energies, such a He atom can be absorbed by He-bubble, resulting in its growth. After the absorption of each He atom, the system is relaxed for 5 ps under the constant number of atoms N, volume V, and temperature T (NVT) ensemble before the next He atom is inserted. The temperature is controlled by Nose-Hoover thermostat.[31] The time step is 0.5 fs for all MD simulations. The visualization of the simulation results is done by OVITO program[32] and AtomEye.[33] The Voronoi method is used to analyze the volume of atom cell.

Grain boundary energy (GBE) is defined as the energy difference between the system before and after the formation of GB. Thus, GBE is calculated by the same method in Ref. [23] as follows:

$$GBE = \sum_i (E_i - E_\mathrm{p})/A, \tag{1}$$

where E_i and E_p are the potential energy of atom in grain boundary and bulk crystal respectively, and A is the GB's area in the x–y plane. The calculation is done in the middle 40 atomic layers, in order to eliminate size effect and thus only one GB is considered for the GBE calculation. Our pre-testing also has confirmed that the energy difference between the adjacent atomic layers is small enough after 40 atomic layers away from GB plane. In addition to the GBE, the largest free volume

within a grain boundary is another useful parameter to estimate the property of GB, which is defined as the largest spherical volume inserted between atoms within the GB region.[15]

The stress and pressure for each of He and W atoms are calculated from Eqs. (2) and (3) as follows:

$$\sigma_{\alpha\beta}(i) = \frac{1}{V_i}\left(\frac{1}{2}\sum_i F_{ij}^{\alpha} r_{ij}^{\beta} + m_i v_i^{\alpha} v_i^{\beta}\right), \tag{2}$$

$$P(i) = -\frac{1}{3}(\sigma_{xx}(i) + \sigma_{yy}(i) + \sigma_{zz}(i)), \tag{3}$$

where V_i is the current Voronoi volume of atom i; α and β are the Cartesian components; F_{ij} is the force on the atom i due to atom j; r_{ij} is the vector coordinate of neighbor atom j relative to atom i; m_i is the mass of atom i; v_i is the velocity of atom i, $P(i)$ is the pressure of atom i; σ_{xx}, σ_{yy}, and σ_{zz} are the stress components in the x, y, z directions, respectively.

In addition to the above properties, the potential energy difference between the W-matrix before and after the formation of He bubbles is also calculated from the following equation:

$$\delta E = E_{\mathrm{W}}(\mathrm{He-bubble}) - E_{\mathrm{W}}(\mathrm{ref}), \tag{4}$$

where δE is the potential difference; $E_{\mathrm{W}}(\mathrm{He-bubble})$ and $E_{\mathrm{W}}(\mathrm{ref})$ are the potential energy of W atoms in GB before and after the formation of He bubble. With this equation, the distortion of lattice structure and related pressure can be qualitatively determined as explained in Subsection 3.4.

The average formation energy of He bubble is shown as a function of bubble size. The average formation energy of the bubble is defined as[34]

$$E_{\mathrm{ave}}^{\mathrm{f}}(n) = \left[E_{\mathrm{bubble}}(n) - E_{\mathrm{bulk}} - nE_{\mathrm{He}}\right]/n, \tag{5}$$

where $E_{\mathrm{bubble}}(n)$ is the total energy of simulation supercell containing n He atoms in the bubble; E_{bulk} is the total energy of the super-cell without the bubble; E_{He} is the cohesive energy of closely packed He, which is 0.0054 eV.[29,30]

To evaluate the stability of He bubble at GB, we have also defined the average binding energy of each He atom in the He bubble, which is defined as[35]

$$E_{\mathrm{ave}}^{\mathrm{b}}(n) = \left[nE^{\mathrm{f}}(\mathrm{He}) - E^{\mathrm{f}}(n)\right]/n, \tag{6}$$

where $nE^{\mathrm{f}}(\mathrm{He})$ is the sum of the formation energy of n discrete He atoms dissolved separately in tetrahedral interstitial sites in perfect W, and $E^{\mathrm{f}}(n)$ is the formation energy of He bubble, which is equal to $nE_{\mathrm{ave}}^{\mathrm{f}}(n)$. The positive average binding energy indicates the attractive interaction between He atom and grain boundary in this paper.

The average-volume of He atoms in the He bubble is defined as

$$V = \frac{\sum_i^N V_{\mathrm{He}-i}}{N}, \tag{7}$$

where $V_{\mathrm{He}-i}$ is the current Voronoi volume of He atom i in the He bubble and N is the number of He atoms in He bubble.

3. Results and discussion

3.1. Grain boundary structure and energy

The structure of the HAGBs after full relaxations before the insertion of He atoms is shown firstly in Fig. 1. From Fig. 1(a), it is clear that the arrangement of atoms in the GBs of high-angle twist grain boundaries is still kept after the complete relaxation, which is different from that in the symmetrical grain boundaries of $\Sigma3\{111\}[1\text{-}10]$ and $\Sigma5\{012\}[100]$.[15] Viewing along the [110] direction, the lattice atomic arrangements at 20° and 40°-rotated GBs (20°-GB, 40°-GB) are disordered, while the 70.53°-rotated GB (70.53°-GB) is in good lattice matching as shown in Figs. 1(b)–1(d). The periodic patterns are observed in HAGBs. In this work, a pattern containing one or more W atoms with potential energy greater than −10.4 eV is defined as a dislocation-junction as shown in Figs. 1(b) and 1(c), while a continuous pattern in which all W atoms with potential energy greater than −10.7 eV is defined as a dislocation-band as shown in Fig. 1(d).

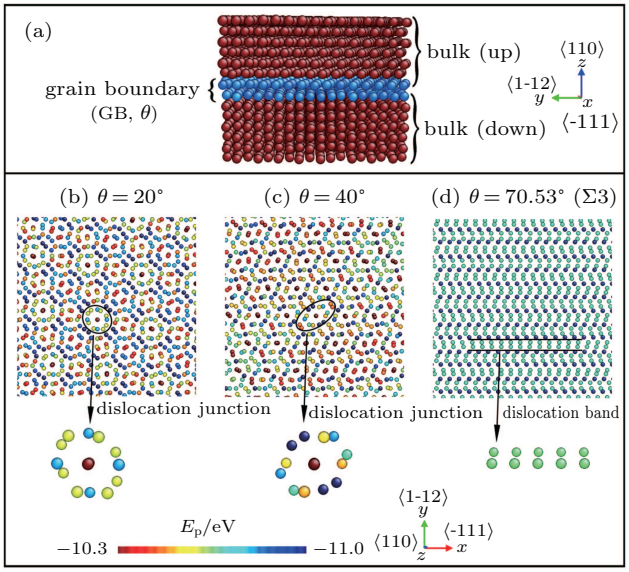


Fig. 1. (a) Structure of twist grain boundary viewed along [-111] direction. Blue atom: GB; dark red atom: bulk. (b)–(d) Dislocation-junction and dislocation-band distribution on GB plane along [110] direction for $\theta = 20°$ (b), 40° (c), and 70.53° (d) (Σ3). Atoms are colored according to potential energy, as indicated by the color bar.

In Fig. 2, the density of dislocation junctions at 40°-GB is the highest, followed by 20°-GB and the lowest density appears at 60°-GB. The distribution of dislocation junctions is uniform for 20°-GB and 40°-GB. There is no dislocation-junction at 70.53°-GB, and the potential energy of lattice atom in the dislocation-band at 70.53°-GB is relatively low. Further analysis of other high angle twist grain boundaries (*e.g.*, 30°-GB, 90°-GB) also indicates that they have similar struc-

tural characteristics to the dislocation-junctions or dislocation-bands that are periodically distributed. Therefore, from the analysis of dislocations-junction or dislocations-band's density and the change of the grain boundary energy (listed in Table 1), it can be concluded that the grain boundary with high-density high-energy dislocation-junctions or dislocation-bands has higher grain boundary energy (GBE).

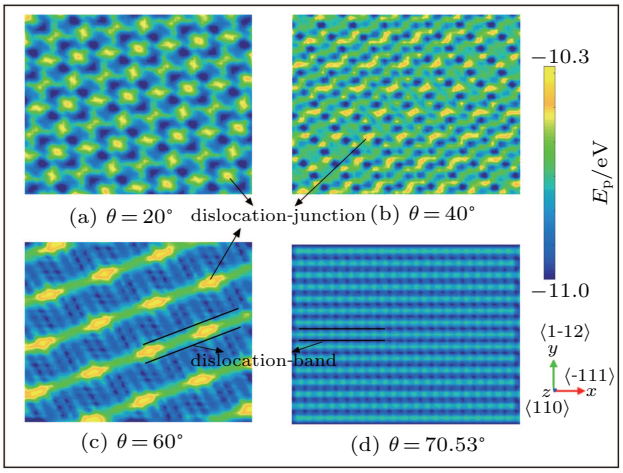


Fig. 2. Density distribution of dislocation-junctions and dislocation-bands on GB plane. The grid dots are colored according to potential energy (a)–(d), as indicated by the color bar. The view direction is along [110].

Table 1. Values of lattice constant (a_0), elastic constants (C_{11}, C_{12}, C_{44}), potential energy (PE), largest free volume (FV), and energy barrier of He atom migration (E_m) between the octahedral sites, obtained by using interatomic potentials.

a_0/Å	C_{11}/GPa	C_{12}/GPa	C_{44}/GPa	PE/eV	FV/Å^3	E_m/eV
3.1805[a]	517[a]	198[a]	142[a]	–11.0	16.84	0.48

[a] Ref. [29].

Table 2. Values of grain boundary energy, largest free volume of different GBs, and the migration energy barrier between dislocation-junctions and dislocation-bands.

θ/(°)	GBE/(eV/Å^2)	FV/Å^3	E_{m1}/eV	E_{m2}/eV
20	8.61	37.15	1.845	–
26.53	8.86	37.70	1.685	–
30	9.05	35.60	1.440	–
34.38	9.27	37.13	1.620	–
38.94	9.15	36.06	1.590	–
40	9.18	35.56	1.567	–
43.38	9.07	36.09	1.460	–
50.48	8.31	36.62	1.230	1.12
54.11	8.45	36.70	1.180	–
60	8.10	35.77	1.200	2.10
65	7.10	35.04	1.700	2.23
70.53	5.68	31.00	1.450	1.45
80	7.87	35.40	1.750	–
90	8.46	36.10	1.576	–

In addition to the above structural and energy results, the loss of symmetry at the GB is expected to result in larger free volume[15] according to the definition of free volume (FV). Thus, the calculation of the FV at GBs is also performed. The values of FV at dislocation-junctions or dislocation-bands are larger than those in other regions of the same GB. The maximum values of FV of dislocation-junctions or dislocation-bands at HAGBs are shown in Table 2. It should be noted that the FV of 70.53°-GB is 31.06 Å^3 which is much lower than those of other grain boundaries. For the GB with higher grain boundary energy, the larger values FV are also observed.

3.2. Migrations of He atoms in grain boundary

From the above analysis, it is clear that periodic dislocation-junctions or dislocation-bands exist in HAGBs. The size of free volume at dislocation-junction is larger than those at other locations. Because of high binding energy of He atom to vacancy-type defects,[36,37] He atoms are expected to be easily trapped by the dislocation-junctions or dislocation-bands first, and the migrations between the junctions or bands form larger-sized He bubbles. Therefore, the NEB method is used to calculate the energy barrier of He migration between the neighboring trapping sites in the twist grain boundary. The results are shown in Fig. 3 and Table 2. For 40°-GB, during the migration of He atom, the saddle point states are located in the regions with small free volume and the energy barrier is around 1.59 eV as shown in Fig. 3(a). Further investigation shows that the 20°-GB, 38.94°-GB, and 90°-GB, *etc.* have the similar energy barriers and diffusion paths. As for 50.48°-GB, the energy barrier is smaller than that at 40°-GB and the two possible paths have values of 1.23 eV (E_{m1}) and 1.12 eV (E_{m2}) respectively. The free volume of the region where the saddle point states are located is also larger than that at 40°-GB between the dislocation-junctions. From Fig. 3(b), it can be found that there is a migration channel with large free volume ($FV = 31.5$ Å^3) between two dislocation-bands at 50.48°-GB. The migration energy of He atoms along this migration channel is small. The similarly migration channels between dislocation-junctions and dislocation-bands are also found at 54.11°-GB and 60°-GB with relatively low energy barrier ($E_m \leq 1.3$ eV) as listed in Table 2. Unlike the migration of He atom in the same band, the migration energy barrier of He atom between adjacent bands is found to be even higher for some GBs as shown in Figs. 2(d) and 2(e). From the above analysis, it can be found that the migration energy depends on the structure of the grain boundary, especially the distribution of free volumes along the migration path in HAGBs. It should also be noted that for the special boundaries (*e.g.*, Σ3), as shown in Fig. 3(c), the energy barrier between dislocation-junctions and that between dislocation-bands are the same due to the good symmetry and lattice matching. All these results indicate that the high diffusion barrier should be one of the reasons for the suppression of initial growth of He bubbles in nanolayered composites.[38]

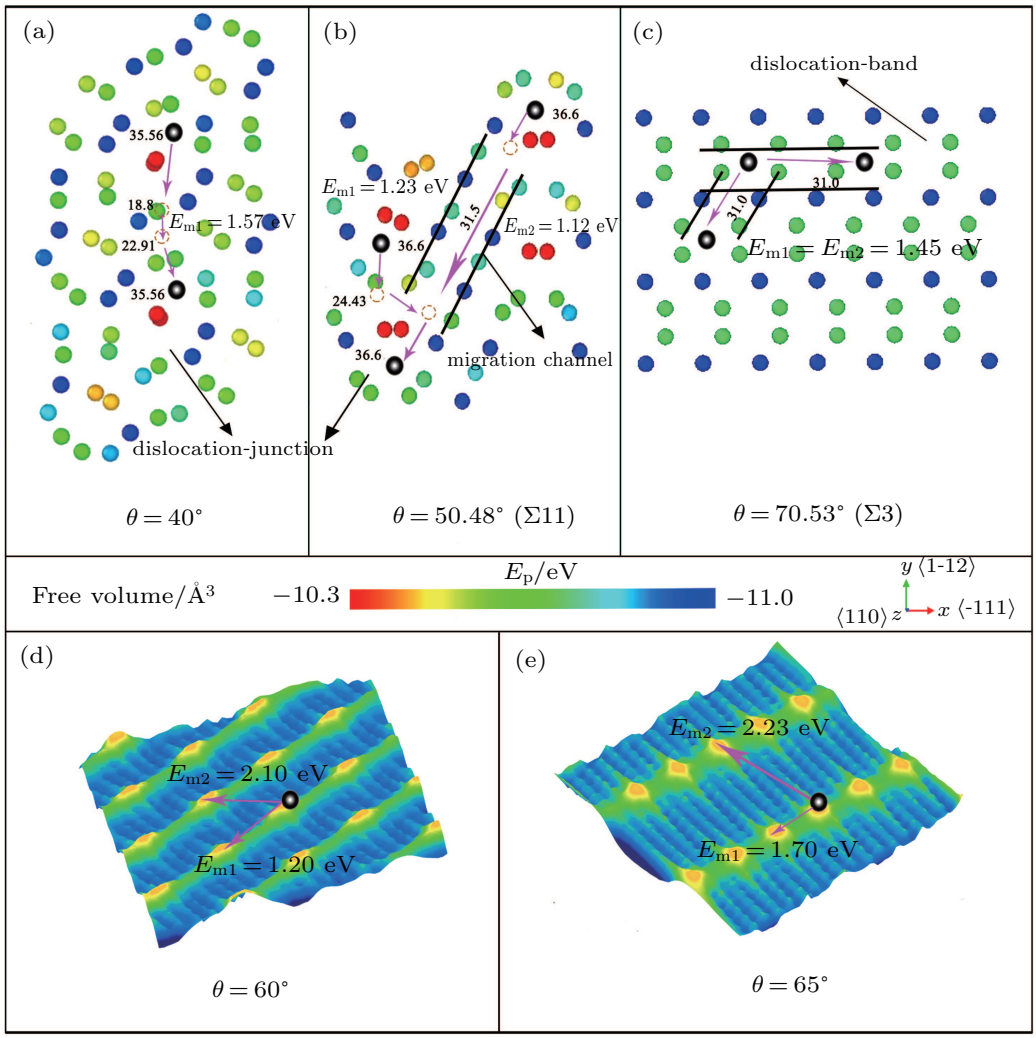


Fig. 3. Migration energy barrier between dislocation-junctions and between dislocation bands. Value along arrow represents size of free volume. Atoms are colored according to potential energy as indicated by color bar. View is along [110] direction.

3.3. He bubble growth in grain boundary

After studying the migration of He atom into He bubble, the evolutions of He bubbles at 20°-GB, 40°-GB, and 70.53°-GB plane are depicted in Fig. 4. The W atoms are first pushed out in the direction of dislocation-junctions when the He bubbles are small clusters as shown in Figs. 4(a), 4(d), and 4(g). As bubble grows into a certain size (Figs. 4(b), 4(e), and 4(h)), the region of grain boundary around the He bubble forms an ordered crystal structure at 20°-GB and 70.53°-GB or a disordered crystal structure at 40°-GB. With the increase of the size of He bubbles (Figs. 4(c), 4(f), and 4(i)), the ordered crystal structure is also expanded at 20°-GB and 70.53°-GB. However, there is still no obvious ordered crystal structure at 40°-GB with He bubble growing. The further analysis indicates that at the atom layer without He bubble in GB plane, the potential energy of the W atom in the ordered crystal structure is lower than that of the other regions as shown in Figs. 4(j) and 4(k). Figure 5 shows the displacement of W atoms in GB plane during the nucleation of He bubble, in which only the W atoms are shown. For 20°-GB, the displacement of W atoms along a certain direction[1–19] leads to the transformation of the local grain boundary structure from disordered crystal structure to ordered crystal structure. However, at 40°-GB, the W atoms are displaced in all directions around the bubble, which is then difficult to form ordered crystal boundaries. For 70.53°-GB, as the number of He atoms increases ($N = 15$), the [-111] dislocation-band continues to absorb displaced W atoms, resulting in the formation of partially ordered crystal boundary on the [-111] dislocation-band. When He bubble grows into a bubble with a certain size ($N = 45$), the He bubble grows along the [1-12] dislocation-band and enters into another dislocation-band, thus further enlarging the ordered crystal boundary. The further investigation shows that there are also a partially ordered structure at 50.48°-GB, 60°-GB, and 90°-GB, while no obvious ordered structure can be formed at 38.94°-GB during the growth of He bubble. Furthermore, the structure at 70.53°-GB has the largest local ordered structure with the same number of He atoms.

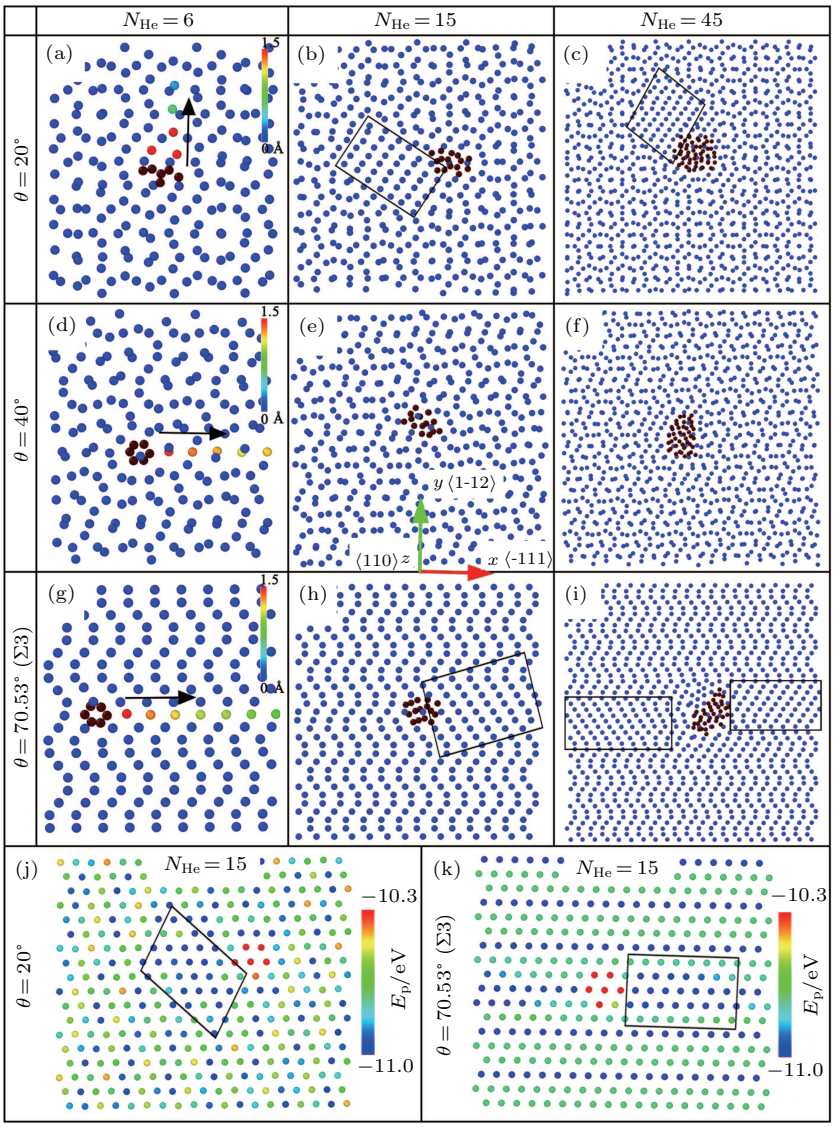


Fig. 4. Evolution of He bubbles at HAGBs. Atoms are colored according to magnitude of displacement in panels (a), (d), and (g) as indicated by color bar. Arrows represent displacement direction. In panels (a)–(i), the Bule atom are W, and dark red atoms are He. In panels (j) and (k), potential energy of atomic layer without He bubble at GB plane is shown. Atoms are colored according to potential energy as indicated by color bar. View is along [110] direction.

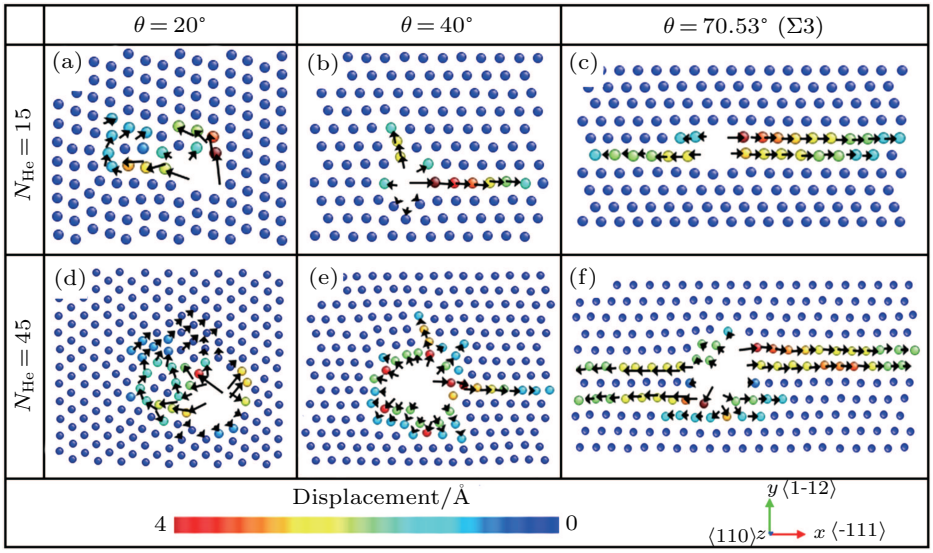


Fig. 5. Displacements of W atoms in the GB plane where He bubbles are located. Arrows represent direction of displacement. Atoms are colored according to magnitude of displacement as indicated by color bar. View is along [110] direction.

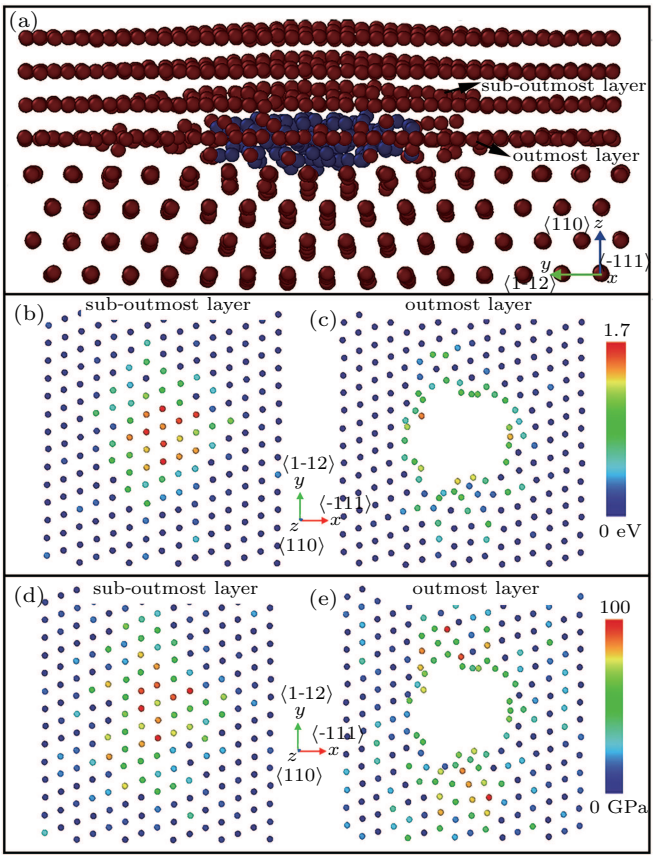


Fig. 6. (a) Bubble with 60 He atoms at 40°-GB. Blue and dark red points are He and W atoms, respectively. View is along [-111] direction. In panels (b)–(e), the potential difference and stress distribution of W atoms after He bubble has formed in sub-outermost and outmost atomic layer are shown. Sub-outermost atomic layers to He-bubble are shown in panels (b) and (d). The outmost atomic layer are shown in panels (c) and (e). Atoms are colored according to potential difference and stress respectively as indicated by color bars. View is done along [110] direction.

3.4. Larger He bubble in GB

With the increase of the number of He atoms ($N = 60$), He bubble grows along the grain boundary with a plate-shape at 40°-GB, which is shown in Fig. 6(a), which is different from the He bubble growing in the bulk[39,40] and in tilt GB.[34,41] It is also clear that with the growth of He bubble, the sub-outmost atomic layers show different behaviors as a function of distance to He bubble. A few W atoms on atomic layer in the upper and lower regions of He bubbles are displaced away from the equilibrium positions, resulting in an arch shape, thuse leaving larger free volume for He bubble. Figures 6(b) and 6(c) illustrate the potential differences between W atoms at the outmost layer and those at sub-outermost layer in the GB after being introduced into the He bubble, which are calculated from Eq. (4). The potential energy difference of atom in sub-outmost atomic layer is greater than that in outermost atomic layer. From these results, it can be found that the larger the potential energy difference, the greater the distortion of lattice structure relative to the equilibrium state is. Therefore, the pressure which He bubble is subjected to from sub-outermost atomic layer is stronger than that from outmost atomic layer as shown in Figs. 6(e) and 6(f). As revealed in Fig. 6(a), the curvature of the bubble near the sub-outermost layer is smaller than that near the out-most layer. Therefore, for the bubble in mechanical equilibrium, the relationship among local-stress, gas-pressure and local-radius of bubble can be formulated by equation[42]

$$P - \sigma = 2\gamma/R, \tag{8}$$

where 2γ is the constant of surface energy; P is the pressure of bubble; $1/R$ is the radius of the curvature of different part of the bubble; σ is the stress which He bubble is subjected to from atomic layer. In this work, we mainly focus on the primary stress acting on the bubble from its near atomic layer. For the sub-outmost atomic layer, such a component of stress is σ_z; for the outmost atomic layer, the components of stress are σ_x, σ_y or σ_{xy}, respectively. It can be seen from Figs. 6(d) and 6(e) that the stress of bubbles subjected to the sub-outmost atomic layer is higher than that subjected to the outermost atomic layer. Therefore, the larger the stress, the higher the curvature radius of the bubble will be, which leads to a plate-shape bubble as shown in Fig. 6(a). Further investigation shows that there are also plate-shape He bubbles at other HAGBs, which suggests that for He bubble nucleation at HAGB in the tungsten, the spherical cluster energetic advantage disappears when the bubble grows.

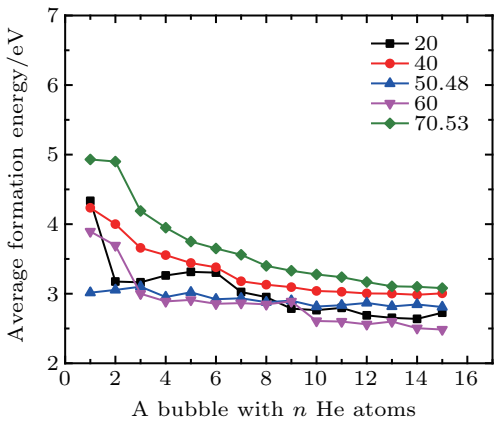


Fig. 7. Plots of average formation energy *versus* bubble with n He atoms in HAGBs for different rotation angles of HAGBs.

In Fig. 7, as the number of He atoms contained in bubble increases, the average formation energy of bubble decreases, and approaches to a constant value when the bubble contains 10 to 15 He atoms. It can also be found that the formation energy of bubble at 70.53°-GB is much larger than that at other HAGBs. Thus, comparing with other grain boundaries, the nucleation of He bubbles at 70.53°-GB is difficult. As shown in Fig. 8, the average binding of bubble increases with the number of He atoms in bubble growing, and also approaches to a constant value when the bubble contains 10 to 15

He atoms. The positive average binding energy indicates that the He atoms will migrate from bulk to the grain boundary, nucleate, and grow into bubble.

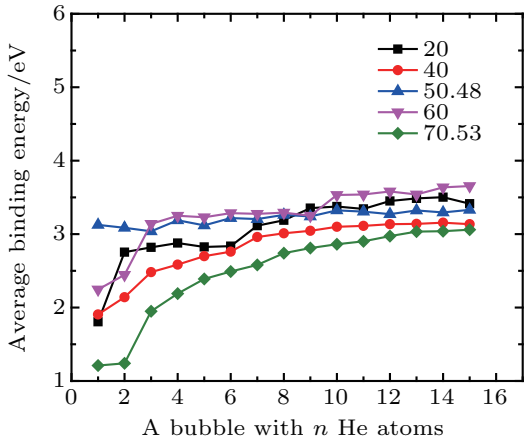


Fig. 8. Plots of average binding energy versus bubble with n He atoms in HAGBs for different rotation angles of HAGBs.

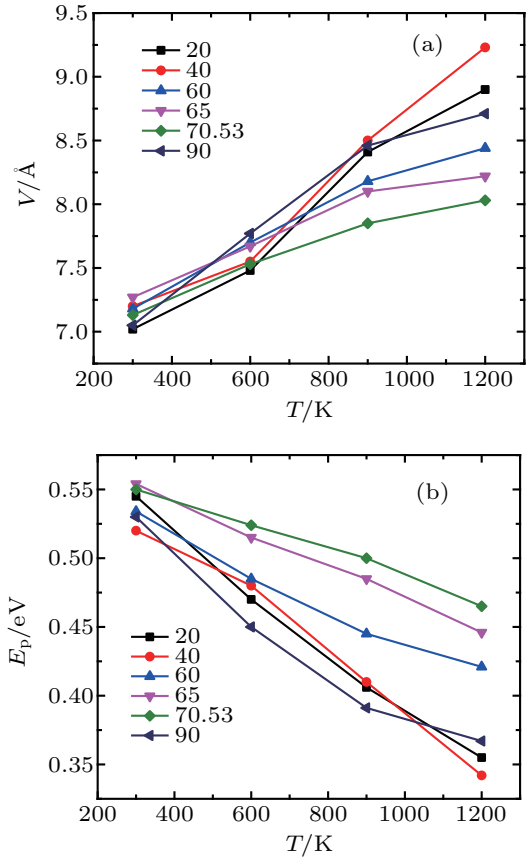


Fig. 9. Plots of (a) average volume and (b) average potential energy of He atoms in bubble *versus* temperature ranging from 300 K to 1200 K for different rotation angles of HAGBs.

We further explore the average-volume of He bubbles ($N = 60$) at different temperatures at different GBs. The results with temperature ranging from 300 K to 1200 K at different twist grain boundaries are shown in Fig. 9(a). It can be found that the volume of gas bubble increases with temperature increasing, while the potential energy of He bubble shows an opposite trend as shown in Fig. 9(b). A similar behavior of He bubbles in the other twist grain boundaries at the temperature ranging from 300 K to 1200 K is also observed. It can be found that the volume of He bubble in high GBE grain boundary is larger than that in low GBE grain boundary at the temperature ranging from 600 K to 1200 K. The linear relationship of average volume with temperature ranging from 600 K to 1200 K can be illustrated in Fig. 9(a). Therefore, by fitting these results, the relationship among the average volume, activation energy and the temperature in a range from 600 K to 1200 K can be determined by the following empirical formula:

$$V = Qk\,(T - 600\ \mathrm{K}) + \mathrm{V}_0, \tag{9}$$

where V is the average volume of He atoms in the He bubble at different temperatures, which can be obtained from formula (7), V_o is the average volume of He atom at 600 K, k is the Boltzmann constant, and Q refers to the activation energy required when the He atom increases its volume, which can be obtained from formula (9). However, the values of the activation energy are different at different grain boundaries. The values of Q are listed in Table 3. The activation energy for the growth of He bubbles in low GBE grain boundary is much larger than that in high GBE grain boundary. From Figs. 9(a) and 9(b), it can be concluded that the high GBE grain boundary will result in larger volume, lower potential energy and more stable He bubble, which is the same as the experimental results obtained in Ref. [43]. Because of high activation energy, it is difficult for He bubble to expand in the low GBE grain boundary when the temperature increases. Meanwhile, for the high GBE grain boundary, the volume of He bubble can be easily increased, which will result in the formation of large-sized He bubble and then cause high-temperature embrittlement of the GBs. Thus, based on the above results, it can be concluded that the formation of large-sized He bubbles in normal high-angle twist grain boundaries is a function of the formation energy, binding energy and migration energy of helium bubbles, which depends on the properties of the GB, *e.g.*, rotation angles and related misfit dislocation patterns.

Table 3. Activation energy required to increase the average volume of He atoms in He bubbles at 20°, 40°, 60°, 65°, 70.53°, and 90° twist grain boundaries.

θ/(°)	20	40	60	65	70.53	90
Q/(eV/Å^3)	3.6×10^{-2}	3.1×10^{-2}	7.0×10^{-2}	9.4×10^{-2}	10.4×10^{-2}	5.5×10^{-2}

4. Conclusions

In this work, the structure of high-angle twist grain boundaries, the migration of He atoms and the growth of He bubbles in HAGBs in W, are investigated by atomic simulations. The results indicate that the loss of the symmetry at the HAGBs can result in forming the patterns of periodic dislocation-junctions, dislocation-bands, and large free volumes. The migration energy barrier between the neighboring trapping sites are calculated by the NEB method, which indicates that migration energy barrier depends on the structure of the grain boundary, especially on the distribution of the free volumes along the migration path in HAGB. The region of grain boundary (GB) around the He bubble can form an ordered or disordered crystal structure, depending on the properties of GB when He bubble grows on GB plane. The He bubbles with plate-shape could be found in HAGBs, which is affected by the stress and potential distribution in the adjacent atomic layers at GB. Furthermore, comparing with the low energy grain boundaries, high energy grain boundaries can result in the formation of the large-sized He bubbles under the condition of high temperature. Therefore, based on the above results, the selection of specific angle of twist grain boundary is a possible way to avoid forming the large-sized He bubbles, and thus preventing or reducing the helium embrittlement in tungsten.

Acknowledgment

We are very grateful to the Information and Network Center of Xiamen University for providing high performance computer.

References

[1] Loarte A, Lipschultz B, Kukushkin A S, Matthews G F, Stangeby P C, Asakura N, Counsell G F, Federici G, Kallenbach A and Krieger K 2007 *Nucl. Fusion* **47** 203
[2] Federici G, Anderl R A, Andrew P, Brooks J N, Causey R A, Coad J P, Cowgill D, Doerner R P, Haasz A A and Janeschitz G 1999 *J. Nucl. Mater.* **266** 14
[3] Federici G, Wuerz H, Janeschitz G and Tivey R 2002 *Fusion. Eng. Des.* **61–62** 81
[4] Huang S L, Ran G, Lei P H, Chen N J, Wu S H, Li N and Shen Q 2017 *Nucl. Instrum. Method B* **406** 585
[5] Huang S L, Ran G, Lei P H, Wu S H, Chen N J and Li N 2016 *Nanomaterials* **6** 210
[6] Trinkaus H and Ullmaier H 1994 *J. Nucl. Mater.* **212–215** 303
[7] Hetherly J, Martinez E, Di Z F, Nastasi M and Caro A 2012 *Scripta Mater.* **66** 17
[8] Wang J, Gao X, Gao N, Wang Z G, Cui M H, Wei K F, Yao C F, Sun J R, Li B S and Zhu Y B 2015 *J. Nucl. Mater.* **457** 182
[9] Elatwani O, Hinks J A, Greaves G, Gonderman S, Qiu T, Efe M and Allain J P 2015 *Sci. Rep.* **4** 4716
[10] Xia M, Guo H Y, Dai Y, Yan Q Z, Guo L P, Li T C, Qiao Y and Ge C C 2018 *Chin. Phys. B* **27** 073103
[11] El-Atwani O, Gonderman S, Suslov S, Efe M, Temmerman G D, Morgan T, Bystrov K, Hattar K and Allain J P 2015 *Fusion. Eng.* **93** 9
[12] Miyamoto M, Mikami S, Nagashima H, Iijima N, Nishijima D, Doerner R P, Yoshida N, Watanabe H, Ueda Y and Sagara A 2015 *J. Nucl. Mater.* **463** 333
[13] Li X C, Shu X, Tao P, Yu Y, Niu G J, Xu Y, Gao F and Luo G N 2014 *J. Nucl. Mater.* **455** 544
[14] Kobayashi R, Hattori T, Tamura T and Ogata S 2015 *J. Nucl. Mater.* **463** 1071
[15] Wang X Y, Gao N, Setyawan W, Xu B, Liu W and Wang Z G 2017 *J. Nucl. Mater.* **491** 154
[16] Bai X M, Voter A F, Hoagl, R G, Nastasi M and Uberuaga B P 2010 *Science* **327** 1631
[17] Chen N, Niu L L, Zhang Y, Shu X, Zhou H B, Jin S, Ran G, Lu G H and Gao F 2016 *Sci. Rep.* **6** 36955
[18] Valles G, González C, Martin-Bragado I, Iglesias R, Perlado J M and Rivera A 2015 *J. Nucl. Mater.* **457** 80
[19] Di Z, Bai X M, Wei Q, Won J, Hoagl, R G, Wang Y, Misra A, Uberuaga B P and Nastasi M 2011 *Phys. Rev. B* **84** 052101
[20] Yang J B, Osetsky Y N, Stoller R E, Nagai Y and Hasegawa M 2012 *Scripta Mater.* **66** 761
[21] Bulatov V V and Cai W 2002 *Phys. Rev. Lett.* **89** 115501
[22] Wang X X, Niu L and Wang S 2017 *J. Nucl. Mater.* **487** 158
[23] Feng Y X, Shang J X, Liu Z H and Lu G H 2015 *Appl. Surf. Sci.* **357** 262
[24] Feng Y X, Shang J X and Lu G H 2017 *J. Nucl. Mater.* **487** 200
[25] Hirel 2015 *Phys. Comm.* **197** 212
[26] Yang J B, Nagai Y, Hasegawa M and Osetsky Y N 2010 *Philos. Mag.* **90** 991
[27] Gao N, Ghoniem A, Gao X, Luo P, Wei K and Wang Z 2014 *J. Nucl. Mater.* **444** 200
[28] Plimpton S 1995 *J. Comput. Phys.* **117** 1
[29] Juslin N and Wirth B D 2013 *J. Nucl. Mater.* **432** 61
[30] Wood M A and Thompson A P 2017 arXiv: 1702.07042 [physics.comp-ph]
[31] Hoover W G 1985 *Phys. Rev. A* **31** 1695
[32] Stukowski A 2010 *Modell. Simul. Mater. Sci. Eng.* **18** 015012
[33] Li J 2003 *Modell. Simul. Mater. Sci. Eng.* **11** 173
[34] Liu X Y, Andersson D A 2015 *J. Nucl. Mater.* **462** 8
[35] Zhao S Q, Ran G, Li F B, Deng H Q and Gao F 2019 *J. Nucl. Mater.* **521** 13
[36] He W H, Gao X, Wang D, Gao N, Cui M H, Pang L and Wang Z G 2018 *Comput. Mater. Sci.* **148** 224
[37] Xie H, Xu K, Lu G H, Yu T and Yin F 2017 *J. Nucl. Mater.* **484** 270
[38] Misra A, Demkowicz M J, Zhang X, Hoagl and R G 2007 *JOM* **59** 62
[39] Wang J L, Niu L L, Shu X L and Zhang Y 2015 *Nucl. Fusion* **55** 092003
[40] Xie H, Gao N, Xu K, Lu G H, Yu T and Yi F 2017 *Acta Mater.* **141** 10
[41] Yang L, Gao F, Kurtz R J, Zu X T, Peng S M, Long X G and Zhou X S 2015 *Acta Mater.* **97** 86
[42] Yu J N 2003 *Irradiation Effect Materials* (Beijing: Chemical Industry Press) pp. 453–455
[43] Thorsen P A, BildeS ørensen J B and Singh B N 2004 *Scr. Mater.* **51** 557